RSC Advances

PAPER

View Article Online
View Journal | View Issue

Cite this: *RSC Adv.*, 2022, **12**, 389

Li@C_{60} thin films: characterization and nonlinear optical properties†

Mathias Wolf, [a] Shuichi Toyouchi, [a]‡ Peter Walke,§[a] Kazuki Umemoto, [b] Akito Masuhara, [b] Hiroshi Fukumura, [c] Yuta Takano, [d] Michio Yamada, [e] Kenji Hirai, [d] Eduard Fron[a] and Hiroshi Uji-i*[adf]

Received 2nd November 2021
Accepted 15th December 2021

DOI: 10.1039/d1ra08051b

rsc.li/rsc-advances

Organic materials have attracted considerable attention in nonlinear optical (NLO) applications as they have several advantages over inorganic materials, including high NLO response, and fast response time as well as low-cost and easy fabrication. Lithium-containing C_{60} (Li@C_{60}) is promising for NLO over other organic materials because of its strong NLO response proven by theoretical and experimental studies. However, the low purity of Li@C_{60} has been a bottleneck for applications in the fields of solar cells, electronics and optics. In 2010, highly purified Li@C_{60} was finally obtained, encouraging further studies. In this study, we demonstrate a facile method to fabricate thin films of Li@C_{60} and their strong NLO potential for high harmonic generation by showing its comparatively strong emission of degenerate-six-wave mixing, a fifth-order NLO effect.

Introduction

Nonlinear optics (NLO) provides a variety of applications such as optical signal processing, ultrafast switches, sensors and creation of correlated photon pairs.[1–5] In order to observe NLO effects, strong electric fields, typically from ultrashort pulsed lasers, are required. Aside from this condition, the choice of material also plays a deciding role as the optical nonlinearities of the material determine the size of the NLO response. Current materials used in NLO are often inorganic like beta-barium-borate (BBO) or gallium arsenide (GaAs).[6,7] These materials have some advantages, such as environmental stability, mechanical strength and a high stability over a large temperature range.[6,7] On the other hand, organic materials are typically superior in terms of having large nonlinear properties, high optical damage thresholds, fast response times and flexibility in terms of engineering their structures.[6,7] C_{60} has been suggested as a promising material for applications in high harmonic generation and ultra-fast optics.[8,9] Fullerenes allow a variety of modifications to alter or enhance their properties. These modifications can be generally divided into two categories: endohedral and exohedral.[10,11] Endohedral modification of C_{60} involves the incorporation of atoms/ions or small molecules into C_{60}. Among those, lithium containing C_{60} (Li@C_{60}) is an interesting candidate for NLO applications. Campbell *et al.* have studied its NLO properties by using mixed C_{60}/Li@C_{60} films.[12,13] They have been able to show an increased NLO response of Li@C_{60} compared to ordinary C_{60} and found a response comparable to other favorable organic molecules.[12,13] One problem that remained was the low purity of the samples as Li@C_{60} was mixed with ordinary C_{60}. However, in 2010 Aoyagi *et al.* have succeeded in obtaining highly purified Li@C_{60} reaching purities as high as 99%.[14] Increased NLO properties have been theoretically predicted for Li^+@C_{60}(PF_6^-) salt.[15] However, the NLO properties using these high purity samples have not been experimentally examined yet.

In this study, we demonstrate a simple method of obtaining Li@C_{60} thin films and characterize them by using Raman spectroscopy and atomic force microscopy (AFM). We further examine the NLO properties of the Li@C_{60} thin film excited by two distinct femtosecond (fs) pulsed laser beams on an optical microscope with epi-detection configuration. It is found that the Li@C_{60} thin films exhibit strong degenerate-six-wave mixing (DSWM), a fifth-order nonlinear optical effect with high reproducibility thanks to the high purity, marking it as a strong candidate for high-harmonic generation (HHG).

[a]*Division of Molecular Imaging and Photonics, Department of Chemistry, KU Leuven, Celestijnenlaan 200F, 3001 Leuven, Belgium. E-mail: hiroshi.ujii@kuleuven.be*

[b]*Graduate School of Science and Engineering, Yamagata University, Yonezawa, Yamagata 992-8510, Japan*

[c]*Department of Chemistry, Graduate School of Science, Tohoku University, 6-3 Aramaki, Aoba, Sendai, 980-8578, Japan*

[d]*RIES, Hokkaido University, N20W10, Kita-Ward, Sapporo, Japan*

[e]*Department of Chemistry, Tokyo Gakugei University, Nukuikitamachi 4-1-1, Koganei, Tokyo 184-8501, Japan*

[f]*Institute for Integrated Cell-Material Science (WPI-iCeMS), Kyoto University, Yoshida, Sakyo-ku, Kyoto 606-8501, Japan*

† Electronic supplementary information (ESI) available. See DOI: 10.1039/d1ra08051b

‡ Present address: Department of Applied Chemistry, National Yang Ming Chiao Tung University, 1001 Ta Hsueh Rd., Hsinchu 30010, Taiwan.

§ Present address: Department of Materials and Environmental Technology, Tallinn University of Technology, Ehitajate tee 5, 19086 Tallinn, Estonia.

Experimental

Sample preparation

$Li^+@C_{60}(PF_6^-)$ powder purified through recrystallization was purchased from Idea International Co. Ltd. Thin films of $Li@C_{60}$ have been produced by simple dropcasting from a saturated *o*-dichlorobenzene (DCB) solution of $Li^+@C_{60}(PF_6^-)$ in the presence of a trace amount of sodium chloride (NaCl) or sodium iodide (NaI) on a cleaned glass coverslip. C_{60}–Ad films have been prepared by dropcasting from toluene solution of C_{60}–Ad[16] in toluene (0.5 mg mL^{-1}). C_{60} films have been prepared following a reprecipitation method outlined by Masuhara *et al.*[17] Shortly, C_{60} is dissolved in *m*-xylene (good solvent) and subsequently injected into ethanol (poor solvent).

Methods

Nonlinear optical (NLO) measurements and Raman spectroscopy were performed using an inverted optical microscope (Ti-U, Nikon) equipped with an OmegaScope 1000 for Atomic Force Microscopy (AFM) measurements. Observation of films by scanning electron microscope (SEM) was performed by Hitachi SU8230. Energy-dispersive X-ray spectroscopy (EDX) under SEM observation was performed by Bruker Quantax EDS. For NLO, the sample was illuminated by fs pulses at 820 nm (Mai Tai HP, Spectra-Physics, 120 fs, 80 MHz) and 1164 nm (Inspire HF 100, Spectra-Physics, 200 fs, 80 MHz, pumped by Mai Tai HP) focused by an objective lens (60x, Plan Apo, air, NA 0.95, Nikon). Temporal overlap of the two wavelengths has been achieved using a delay line that allows precise adjustment of the 820 nm beam path length. The laser pulses were directed to sample with a shortpass dichroic mirror (T750spxrxt, Chroma Technology Corporation). In order to block excitation light, a 750 short-pass (ET750sp, Chroma) was used. The fitting of NLO intensity depending on power has been done using "curve_fit" included in Python's scipy library. For Raman spectroscopy, a 633 nm laser (Research Electro-Optics, Inc.) was focused on samples with a 60x Plan Fluor objective (NA 0.85, Nikon). The laser was reflected by using a longpass dichroic mirror (ZT633rdc, Chroma Technology Corporation). To block excitation laser light, a 645 long-pass (HQ645LP, Chroma Technology Corporation) was used. The backscattered NLO and Raman signals were collected by the respective objectives used for excitation and spectra were recorded using a spectrograph (iHR320, HORIBA) equipped with a charge-coupled device (CCD) camera (Newton DU920P, Andor Technology Ltd). NLO/Raman signal from out of focus was removed by a pinhole (diameter 100 μm). AFM data was analyzed using Gwyddion.[18]

Results and discussion

$Li@C_{60}$ thin film characterization

$Li@C_{60}$ films have been made using a simple dropcasting method. 30 μL of a saturated solution of dichlorobenzene (DCB) containing $Li^+@C_{60}(PF_6^-)$ (purity 91%) and NaCl or NaI were dropped on a cleaned glass coverslip. Previous studies of $Li@C_{60}$ thin films have primarily used sublimation under ultra-high vacuum (UHV) to obtain thin films.[19–22] In contrast to this conventional method, the approach presented here offers an easy and quick alternative that does not require UHV. After evaporation of the solvent, long-stretched films can be clearly observed on the surface in an optical transmission microscope image (Fig. 1a). To further investigate these films, Raman spectroscopy and AFM measurements have been carried out. The characteristic Raman spectrum of C_{60} can be clearly observed (Fig. 1b). An interesting feature is found when taking a closer look at the $A_g(2)$ mode of C_{60} that is typically positioned at 1470 cm^{-1} for ordinary C_{60}.[23] In the case of $Li@C_{60}$ films, the $A_g(2)$ mode peak is shifted to 1466 cm^{-1}. This is in good agreement with $Li^+@C_{60}[PF_6^-]$ powder and means a shift compared to C_{60} powder by 3 cm^{-1} (see Fig. S5†). Experiments with potassium/calcium-doped C_{60} have shown that the origin of this shift can be traced to negative charge on the fullerene cage.[24,25]

AFM measurements (Fig. 1c and d) reveal a small thickness of a range of 10–20 nm for these films. The thickness falls into the nanoscale region and is advantageous for epi-detecting of NLO signals. In case of four-wave mixing (FWM) and second-harmonic generation (SHG) the phase matching condition is typically only fulfilled in the forward direction but this is different for objects in the nanoscale region. For nanoscale objects, the phase matching condition is usually fulfilled in both forward and backward direction instead of just the forward direction making detection of NLO phenomena easier.[26,27] This can be an advantage for later applications as designs can be more versatile in terms of excitation and detection directions. Taking advantage of the nanoscale structure, such thin films have been thus used in THz applications and ultra-fast information processing.[1,28] EDX mapping under SEM observation was performed to chemically analyze the films formed using NaI as a salt. The long-stretched film was visualized by SEM, which is in good agreement with the AFM analysis (Fig. 2a, see S6† for additional SEM images). It can be seen from Fig. 2b–d that the films contain mainly carbon, phosphorus and fluorine, meaning the films are composed of $Li@C_{60}$ and PF_6 (see Fig. S7† for full EDX spectrum). On the other hand, sodium and iodine are not present in the films, meaning the salt is not directly involved in the film formation (Fig. 2e and f). If no salt was added to the solution, however, film formation was not observed at room temperature under ambient conditions. It is well known that salts can slow down the evaporation of a solvent since they increase the energy necessary for evaporation. If $Li@C_{60}$ and PF_6 films form slowly, a slow evaporation of the solvent would be necessary to see film formation. To check if such a factor was at play here, we cooled a solution without salt down for about 5 min in a freezer (−18 °C) and dropcasted the cold solution onto a coverslip. Cooling the solution is meant to simulate the effect of salt slowing down the evaporation of the solvent. As can be seen in Fig. S8,† film formation could be observed. We further tested the same procedure under cold

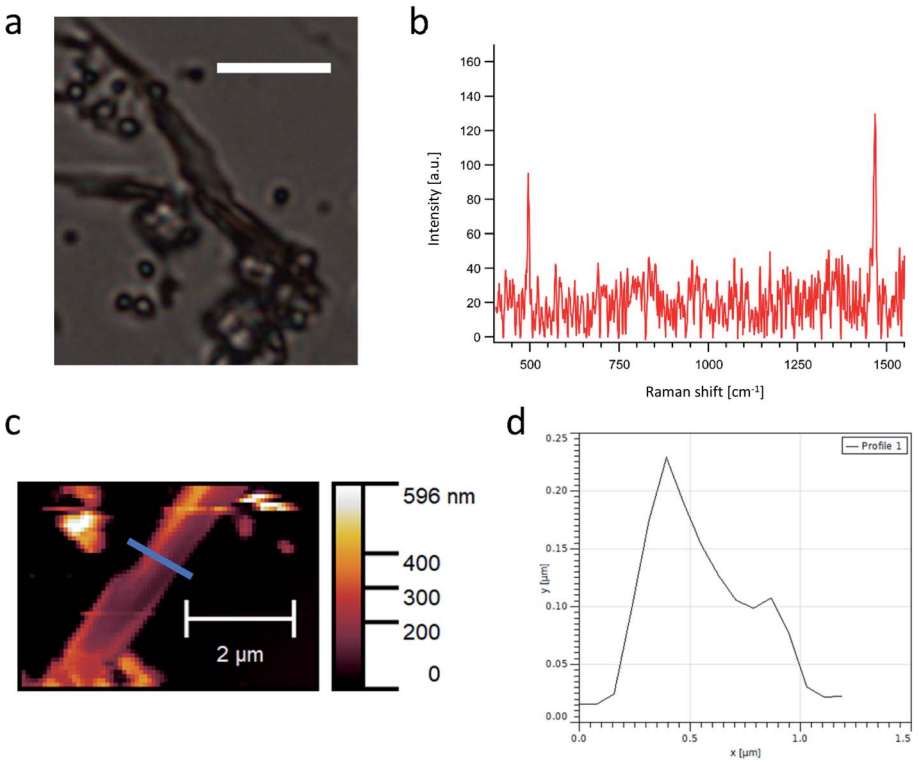

Fig. 1 Li@C_{60} film characterization. (a) Optical transmission microscope image showing the films obtained after dropcasting the Li@C_{60} containing solution on the surface. Scale bar is 5 µm. (b) Raman spectrum obtained from Li@C_{60} film by irradiation with 633 nm laser. The spectrum displays the signature of C_{60}. The spectrum was smoothed using Savitzky–Golay filter and background corrected. (c) AFM image showing the topography of a film formed after dropcasting. (d) Height profile of film shown in (c), position marked by blue line.

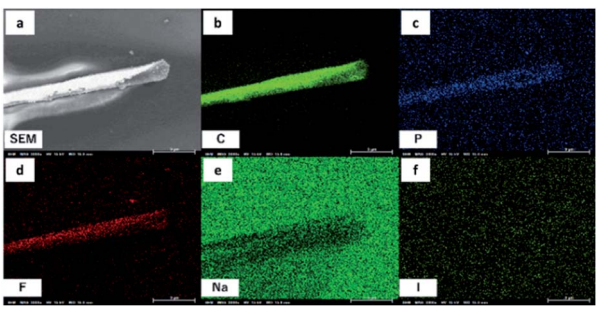

Fig. 2 SEM and corresponding EDX maps showcasing the distribution of various elements of interest. (a) SEM image. (b)–(f) EDX maps showing the distribution of carbon (b), phosphorus (c), fluorine (d), sodium (e) and iodine (f). Scale bars are 9 µm.

conditions with a solution that did contain salt and film formation could be observed with even higher coverage. These results support the aforementioned effect of salt and suggest that Li@C_{60} and PF_6 films form slowly and thus the solvent has to evaporate slowly in order to obtain films. Thus, salt supports film formation by slowing down the evaporation of the solvent.

Nonlinear optical properties of Li@C_{60} thin films

Fig. 3 shows a typical NLO spectrum observed while irradiating the sample with temporally overlapped two coherent fs pulses, *i.e.* pump at 820 nm and Stokes at 1164 nm. The two beams are linearly polarized, parallel to each other. Several NLO signals have been observed from a thin film of Li@C_{60}: SHG (at 582 nm), sum-frequency generation (SFG, at 480 nm), degenerate-FWM (DFWM, at 630 nm) as well as a peak at roughly 455 nm that cannot be explained with just second or third order nonlinear optical effects. Degenerate six-wave mixing (DSWM),

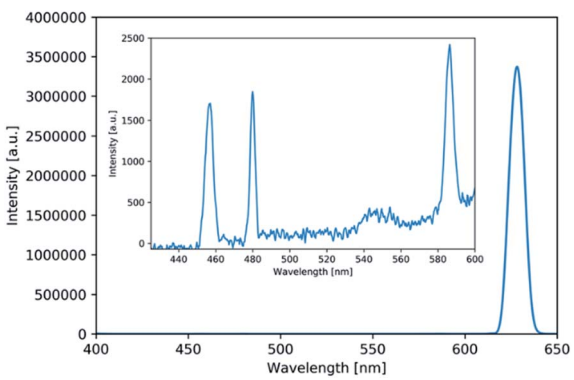

Fig. 3 Spectrum obtained by irradiating a Li@C_{60} film with fs pulses at 820 nm and 1164 nm. Inset shows a zoomed in view of the spectrum from 425 to 600 nm. The peaks observed are DFWM (630 nm), SHG (582 nm), SFG (480 nm) and DSWM (455 nm). Peak power densities are 19.7 GW cm^{-2} (820 nm) and 22.5 GW cm^{-2} (1164 nm).

a higher order nonlinear effect, can be generated at the frequency $4\omega_s - \omega_p$ with the wave vector $4k_s - k_p$, where ω_i and k_i (i = s or p) represent frequency and wave vector of Stokes or pump light, respectively. Converting 820 nm and 1164 nm wavelengths to their frequencies that are roughly 3.66×10^{14} Hz and 2.58×10^{14} Hz, respectively, we can see that

$$4 \times 258\ \text{THz} - 1 \times 366\ \text{THz} = 666\ \text{THz} \mathrel{\hat{=}} 451\ \text{nm} \quad (1)$$

This calculation suggests that the observed peak around 455 nm is in fact DSWM, a fifth-order NLO effect. The small deviation from the actual peak position can be explained by fluctuations in the output wavelength of the Stokes beam.

In order to experimentally confirm that the observed effect can be attributed to a fifth-order process, the power dependence of this effect has been studied. The peak intensity was measured with varying powers of 820 nm and 1164 nm fs pulsed lasers for several films and the results fitted to a power law equation:

$$y = ax^b \quad (2)$$

In this case, y is the intensity of the signal, x the input power, b depends on the number of photons involved in the process, while a is a constant. The results from two separated measurement sessions are displayed in Table S1.† The measurements show that the intensity of the 455 nm peak depends on the 1164 nm beam to the power of 4 and the 820 nm beam to the power of 1, supporting the above calculation (eqn (1)). The question remains if this is a direct six-wave mixing or a cascade effect meaning two subsequent third-order processes following each other. An example of such a cascade effect has been reported by Pelegati *et al.*, observing cascade coherent anti-Stokes Raman scattering (CCARS).[29] However, CCARS would show a power dependence of 3 for the pump beam and of 2 for the Stokes beam. Furthermore, the difference between the two exciting lasers corresponds to roughly 3604 cm^{-1}, which is not in resonance with any Raman-active vibration of C_{60}. There is still the possibility though of the process consisting of a combination of third-harmonic generation (THG) and FWM, both third-order processes. In order to compare the NLO performance of Li@C_{60} with other C_{60} derivatives, C_{60} films have been made following a method discussed by Masuhara *et al.*[17] as well as thin films of C_{60}–adamantylidene (C_{60}–Ad) by using a similar dropcasting method as for Li@C_{60} (see Fig. S9† for optical microscope images, S10† for Raman spectra). C_{60}–Ad was chosen for its good film formation property as well as having an exohedral modification that allows us to compare NLO performance from both an endohedral and exohedral fullerene. Multiple NLO spectra have been measured for Li@C_{60}/C_{60}–Ad/C_{60}, respectively and each average spectrum was calculated from these. As all three types of films show different average thicknesses (20 nm for Li@C_{60} sample 1 and 10 nm for sample 2, 450 nm for C_{60}, 300 nm for C_{60}–Ad, see Fig. S11, S12, S13 and S14†), the average spectra for DFWM and DSWM have been adjusted by multiplying the spectrum of Li@C_{60} by 22.5/45 (for sample 1 and 2, respectively) and of C_{60}–Ad by 1.5 (using the ratio of thicknesses of C_{60} : Li@C_{60} and C_{60} : C_{60}–Ad, respectively).¶ A factor in NLO microscopy is the difference in emission in forward and backward direction. However, until a sample thickness of roughly half of the excitation wavelength, emission intensity is nearly similar in both directions and increases roughly linearly with the thickness in case of FWM.[26,27] Fig. 4a shows the thickness adjusted DFWM signal. After accounting for the film thickness, DFWM signal from Li@C_{60} come out roughly 8 times as strong as ordinary C_{60}, while C_{60}–Ad shows only a small increase in intensity. Different values have been reported for $\chi^{(3)}$ of C_{60} typically ranging from a magnitude of 10^{-9} to 10^{-12} esu.[9] We predict the value of Li@C_{60} to be roughly one order of magnitude larger compared to ordinary C_{60}, in line with the value reported by Campbell *et al.*[12] The reason for this increase was attributed to a partial charge transfer, which has also been confirmed to happen here as determined from the Raman spectrum when looking at the $A_g(2)$ mode peak shift at 1466 cm^{-1} (Fig. S5†). A striking feature is that SFG is of significant strength for Li@C_{60}, even though it remains weaker than C_{60}–Ad (Fig. 4b). SFG is a second order NLO effect which usually require breaking of centrosymmetry. However, observation of SHG in C_{60} films with significant bulk contribution has been reported[30] despite it being a centrosymmetric molecule and typically having a centrosymmetric bulk structure.[31] It is thus difficult to make quantitative comparisons as the signal is composed of contributions from the surface and the bulk. For Li@C_{60}[PF_6^-] too, a centrosymmetric structure has been reported.[32] Despite C_{60} showing significant bulk contribution at 450 nm thickness,[30] the Li@C_{60} signal is still stronger despite the films being thinner by a factor of more than 22, pointing to its strong enhancement in Li@C_{60}. We will provide reasons why enhancement of second-order effects is expected for Li@C_{60} and C_{60}–Ad in the following section. The breaking of centrosymmetry is obvious for C_{60}–Ad considering its exohedral modification. It is however less obvious for Li@C_{60}. As discussed previously, the Raman spectrum of Li@C_{60} films has shown an $A_g(2)$ mode peak shift by 3 cm^{-1} compared to ordinary C_{60} due to a charge transfer (Fig. S5†). It has been shown that negative charge reduces the degeneracy of HOMO and LUMO of C_{60} as well as its overall symmetry.[33] Additionally, it has been shown that the encapsulated lithium ion is off center, thus causing further symmetry breaking.[14] Symmetry breaking has also been reported for other endohedral fullerenes.[34] The second and strikingly remarkable feature is that DSWM appears the strongest for Li@C_{60} and only weakly for C_{60} and C_{60}–Ad (Fig. 4c) after adjusting for thickness. Since DSWM is a fifth-order effect it does not require breaking of centrosymmetry and can thus be efficiently generated in the bulk, meaning that thickness adjustment is similarly justified as for DFWM. It should be mentioned that for sample 2 of Li@C_{60}, the beam

¶ Polarization dependence is not considered here as it was reported previously that C_{60} films do not show any polarization dependence when rotating linear polarized light in the x,y-plane.[30] As Li@C_{60}[PF_6^-] has a similar structure to C_{60}, we assume a similar situation here.[32] The spectra obtained from Li@C_{60} films, as well as C_{60}–Ad and C_{60} films can be seen in Fig. S15–17† together with further discussion concerning the polarization dependence.

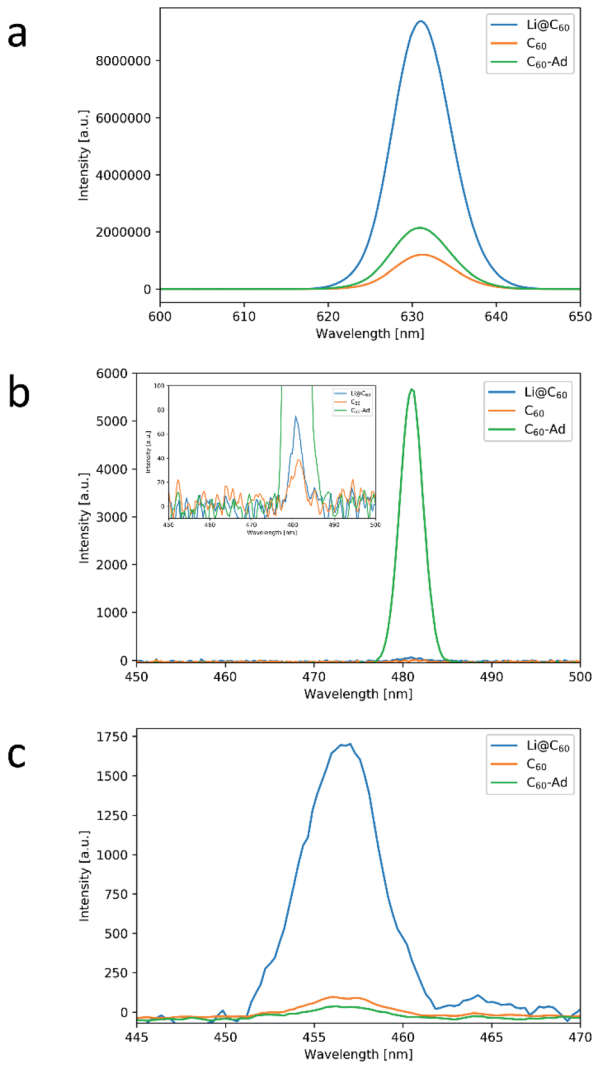

Fig. 4 NLO spectra obtained by irradiation with 820 nm and 1164 nm fs pulses from Li@C_{60} films (blue), C_{60} (orange) and C_{60}–Ad (green). (a) DFWM, thickness adjusted, sample 1. (b) SFG. Inset shows a zoomed in view of the spectrum. (c) DSWM, thickness adjusted, sample 2. Peak power densities were 21.0 GW cm^{-2} (820 nm) and 6.2 GW cm^{-2} (1164 nm) for (a) and (b) and 19.7 GW cm^{-2} (820 nm) and 22.5 GW cm^{-2} (1164 nm) for (c).

spot size is slightly larger than the lateral size of the films meaning some excitation intensity is lost. Assuming a diffraction limited spot size, an objective with an NA of 0.95 means the spot size is roughly 1 μm while the films are typically around 700 nm. However, as the edges of a Gaussian beam have only low intensity and DSWM has a power dependence of 5 on the electric field, we assume that this loss can be neglected. The reason for the increase in intensity is likely due to a partial charge transfer, similar to the case of DFWM. Another possible reason could be its higher absorption in the UV region compared to ordinary C_{60}.[35] Chang *et al.* reported an enhanced emission of THG when the sample showed higher absorption even if no specific electronic transition was affected.[36] C_{60} has been suggested as a promising material for HHG as harmonics can be generated with comparatively low input powers.[8,9] The high strength of DSWM and its higher absorption all the way into the UV region[35] indicates that Li@C_{60} can be an interesting choice for HHG.

Conclusions

In conclusion, we have shown the formation and characterization of thin films made from Li@C_{60} and their NLO response. In particular, we were able to observe DSWM and significant second-order enhancement over ordinary C_{60}. The observation of such high order NLO effects proves the strong NLO properties of Li@C_{60} and makes it is a promising candidate for HHG. This could further improve future X-ray lasers. Furthermore, SWM has been proposed as a way to obtain correlated photon triplets,[37] which could allow further tests of quantum mechanics.

Author contributions

M. W.: conceptualization, methodology, formal analysis, investigation, visualization, writing – original drafts. S. T.: conceptualization, methodology, aupervision, writing – original draft. P. W.: writing – review and editing. K. U.: resources, writing – review and editing. A. M.: resources, writing – review and editing. H. F.: resources, writing – review and editing. Y. T.: resources, writing – review and editing. M. Y.: resources, writing – review and editing. K. H.: methodology, investigation, visualization, writing – original draft. E. F.: resources, writing – review and editing, funding acquisition. H. U.: conceptualization, supervision, writing – original draft, project administration, funding acquisition.

Conflicts of interest

There are no conflicts of interest to declare.

Acknowledgements

This work was supported by the research Foundation – Flanders (FWO, G0D4519N, G081916N) and the KU Leuven Research Fund (C14/15/053, C14/19/079). M. W. would like to thank Ngoc-Uyen Tran, M.Sc., for preparation of the TOC. M. W. acknowledges the FWO PhD-SB fellowship (1S87918N). JSPS Kakenhi (JP19KK0136, JP20K21200, JP17H03003, JP20K21165, JP21H04634), JSPS 'Core-to-Core Program, A. Advanced Research Networks', 'Network Joint Research Center for Materials and Devices' and the Photo-excitonix Project in Hokkaido University are greatly acknowledged. Funding was provided by the European Regional Development Fund and the programme Mobilitas Pluss (MOBJD609). We thank the open facility at Hokkaido University for accessing FE-SEM. H. F. thanks Kazuhiko Kawachi and Yasuhiko Kasama (IDEA international) for various information on synthesis and characterization of Li@C_{60}. The authors want to thank Dr Yasuhiko Kasama (IDEA international) for providing a sample of Li@C_{60}[PF_6^-]. The authors would like to thank Prof. Stijn Van Cleuvenbergen for his valuable advice.

Notes and references

1 J. Y. Wu, Z. A. Li, J. D. Luo and A. K. Y. Jen, *J. Mater. Chem. C*, 2020, **8**, 15009–15026.
2 D. Cotter, R. J. Manning, K. J. Blow, A. D. Ellis, A. E. Kelly, D. Nesset, I. D. Phillips, A. J. Poustie and D. C. Rogers, *Science*, 1999, **286**, 1523–1528.
3 Z. Chai, X. Y. Hu, F. F. Wang, X. X. Niu, J. Y. Xie and Q. H. Gong, *Adv. Opt. Mater.*, 2017, **5**, 1600665.
4 L. Thevenaz, *Front. Optoelectron. China*, 2010, **3**, 13–21.
5 L. Caspani, C. L. Xiong, B. J. Eggleton, D. Bajoni, M. Liscidini, M. Galli, R. Morandotti and D. J. Moss, *Light: Sci. Appl.*, 2017, **6**, e17100.
6 H. S. Nalwa, *Appl. Organomet. Chem.*, 1991, **5**, 349–377.
7 M. Li, Y. Li, H. Zhang, S. Wang, Y. Ao and Z. Cui, *J. Mater. Chem. C*, 2017, **5**, 4111–4122.
8 G. P. Zhang, *Phys. Rev. Lett.*, 2005, **95**, 047401.
9 G. P. Zhang, X. Sun and T. F. George, *J. Phys. Chem. A*, 2009, **113**, 1175–1188.
10 H. Shinohara, *Rep. Prog. Phys.*, 2000, **63**, 843–892.
11 R. Taylor, *C. R. Chim.*, 2006, **9**, 982–1000.
12 E. E. B. Campbell, S. Couris, M. Fanti, E. Koudoumas, N. Krawez and F. Zerbetto, *Adv. Mater.*, 1999, **11**, 405–408.
13 E. E. B. Campbell, M. Fanti, I. V. Hertel, R. Mitzner and F. Zerbetto, *Chem. Phys. Lett.*, 1998, **288**, 131–137.
14 S. Aoyagi, E. Nishibori, H. Sawa, K. Sugimoto, M. Takata, Y. Miyata, R. Kitaura, H. Shinohara, H. Okada, T. Sakai, Y. Ono, K. Kawachi, K. Yokoo, S. Ono, K. Omote, Y. Kasama, S. Ishikawa, T. Komuro and H. Tobita, *Nat. Chem.*, 2010, **2**, 678–683.
15 A. K. Srivastava, A. Kumar and N. Misra, *Phys. E*, 2016, **84**, 524–529.
16 T. Akasaka, M. T. H. Liu, Y. Niino, Y. Maeda, T. Wakahara, M. Okamura, K. Kobayashi and S. Nagase, *J. Am. Chem. Soc.*, 2000, **122**, 7134–7145.
17 A. Masuhara, Z. Tan, H. Kasai, H. Nakanishi and H. Oikawa, *Jpn. J. Appl. Phys.*, 2009, **48**, 050206.
18 D. Nečas and P. Klapetek, *Cent. Eur. J. Phys.*, 2012, **10**, 181–188.
19 H. J. Chandler, M. Stefanou, E. E. B. Campbell and R. Schaub, *Nat. Commun.*, 2019, **10**, 2283.
20 M. Stefanou, H. J. Chandler, B. Mignolet, E. Williams, S. A. Nanoh, J. O. F. Thompson, F. Remacle, R. Schaub and E. E. B. Campbell, *Nanoscale*, 2019, **11**, 2668–2678.
21 Y. Yamada, A. V. Kuklin, S. Sato, F. Esaka, N. Sumi, C. Zhang, M. Sasaki, E. Kwon, Y. Kasama, P. V. Avramov and S. Sakai, *Carbon*, 2018, **133**, 23–30.
22 H. Yagi, N. Ogasawara, M. Zenki, T. Miyazaki and S. Hino, *Chem. Phys. Lett.*, 2016, **651**, 124–126.
23 J. Menendez and J. B. Page, in *Light Scattering in Solids VIII*, ed. M. Cardona and G. Güntherodt, Springer, Berlin, 1st edn, 2000, ch. 2, vol. 76, pp. 27–95.
24 X. H. Chen, X. J. Zhou and S. Roth, *Phys. Rev. B*, 1996, **54**, 3971–3975.
25 J. Winter and H. Kuzmany, *Solid State Commun.*, 1992, **84**, 935–938.
26 J. X. Cheng, A. Volkmer and X. S. Xie, *J. Opt. Soc. Am. B*, 2002, **19**, 1363–1375.
27 R. LaComb, O. Nadiarnykh, S. S. Townsend and P. J. Campagnola, *Opt. Commun.*, 2008, **281**, 1823–1832.
28 M. Jazbinsek, U. Puc, A. Abina and A. Zidansek, *Appl. Sci.*, 2019, **9**, 882.
29 V. B. Pelegati, B. B. C. Kyotoku, L. A. Padilha and C. L. Cesar, *Biomed. Opt. Express*, 2018, **9**, 2407–2417.
30 X. K. Wang, T. G. Zhang, W. P. Lin, S. Z. Liu, G. K. Wong, M. M. Kappes, R. P. H. Chang and J. B. Ketterson, *Appl. Phys. Lett.*, 1992, **60**, 810–812.
31 K. Prassides, H. W. Kroto, R. Taylor, D. R. M. Walton, W. I. F. David, J. Tomkinson, R. C. Haddon, M. J. Rosseinsky and D. W. Murphy, *Carbon*, 1992, **30**, 1277–1286.
32 S. Aoyagi, Y. Sado, E. Nishibori, H. Sawa, H. Okada, H. Tobita, Y. Kasama, R. Kitaura and H. Shinohara, *Angew. Chem., Int. Ed.*, 2012, **51**, 3377–3381.
33 W. H. Green, S. M. Gorun, G. Fitzgerald, P. W. Fowler, A. Ceulemans and B. C. Titeca, *J. Phys. Chem.*, 1996, **100**, 14892–14898.
34 P. M. Felker, V. Vlček, I. Hietanen, S. Fitzgerald, D. Neuhauser and Z. Bačić, *Phys. Chem. Chem. Phys.*, 2017, **19**, 31274.
35 F. Cataldo, D. A. García-Hernández and A. Manchado, *Fullerenes, Nanotubes, Carbon Nanostruct.*, 2019, **27**, 695–701.
36 C. F. Chang, C. H. Yu and C. K. Sun, *J. Biophotonics*, 2010, **3**, 678–685.
37 S. Q. Zhang, W. Li, K. K. Li, Y. M. Li, F. Mu, Y. Feng, Y. Liu and Y. P. Zhang, *Ann. Phys.*, 2020, **412**, 168000.